

# THE POWER SPECTRUM OF RICH CLUSTERS TO SCALES APPROACHING $1000h^{-1}\text{Mpc}$

CHRISTOPHER J. MILLER AND DAVID J. BATUSKI

Department of Physics & Astronomy, University of Maine

*Draft version June 6, 2019*

## ABSTRACT

Recently, there have been numerous analyses of the redshift space power spectrum of rich clusters of galaxies. Some of these analyses indicate a “bump” in the Abell/ACO cluster power spectrum around  $k = 0.05h\text{Mpc}^{-1}$ . Such a feature in the power spectrum excludes most standard formation models and indicates possible periodicity in the distribution of large-scale structure. However, the data used in detecting this peak include clusters with estimated redshifts and/or clusters outside of Abell’s (1958) statistical sample, *i.e.*  $R = 0$  clusters. Here, we present estimations of the redshift-space power spectrum for a newly expanded sample of 545  $R \geq 1$  Abell/ACO clusters which has a constant number density to  $z = 0.10$  in the Southern Hemisphere and a nearly constant number density to  $z = 0.14$  in the Northern Hemisphere. The volume sampled,  $\sim 10^8h^{-3}\text{Mpc}^3$ , is large enough to accurately calculate the power per mode to scales approaching  $10^3h^{-1}\text{Mpc}$ . We find the shape of the power spectrum is linear on scales  $0.02 \leq k \leq 0.10h\text{Mpc}^{-1}$ , with enhanced power over less rare clusters such as APM clusters. The slope here is  $n = -1.4$ . We detect a flattening in the shape of the power spectrum from  $k = 0.02h\text{Mpc}^{-1}$  down to the largest scales we can accurately probe,  $k = 0.009h\text{Mpc}^{-1}$ . The power spectrum is essentially featureless, and we do not detect any significant peak at  $k \sim 0.05h\text{Mpc}^{-1}$ . We compare the shape of the Abell/ACO rich cluster power spectrum to various linear models.

## 1. INTRODUCTION

There has recently been a renewed interest in accurately determining the power spectrum of matter distribution on large scales; in part due to the increased number of clusters with measured redshifts and the large volumes they trace. The power spectrum for the galaxy distribution has been determined many times for many different classes of galaxies. However, most galaxy surveys lack the volume necessary for the accurate quantification of power on large-scales (*e.g.* the Las Campanas Redshift Survey (Lin *et al.* 1996-hereafter LCRS) or the Stromlo-APM survey (Tadros & Efstathiou 1996). A summary of the results from these analyses is that the redshift-space power spectra roughly agree on scales  $\lambda (= 2\pi/k) < 100h^{-1}\text{Mpc}$ . In this region,  $P(k) \propto k^n$  and  $n \sim -2$ . (Of course, the amplitude of the power spectra depends on the species of galaxy examined which provides strong evidence for a luminosity bias). However, on scales  $\lambda > 100h^{-1}\text{Mpc}$ , there is much less agreement. For example, some galaxy species, such as from the LCRS and the Automated Plate Machine (APM) 2d and 3d surveys show a broad flattening around  $k = 0.05h\text{Mpc}^{-1}$  although no distinct maximum can be found within convincing statistical bounds (LCRS; Tadros and Efstathiou 1996; Peacock 1997; Gatzanaga & Baugh 1998). However, Landy *et al.* (1996) find a distinct peak in  $P(k)$  for a 2 dimensional analysis of the LCRS and Broadhurst *et al.* (1990) find a peak near  $\lambda = 130h^{-1}\text{Mpc}$  in a deep pencil beam survey.

Some Abell/ACO cluster analyses also show a peak around  $k \sim 0.05h\text{Mpc}^{-1}$  (Retzlaff *et al.* 1998; Einasto *et al.* 1997-hereafter E97). Yet other cluster analyses only show a smooth turnover in the power spectrum to its scale-invariant form. For instance, the APM clusters, examined by Tadros, Efstathiou and Dalton (1998-

hereafter TED98) show a maximum in  $P(k)$  at the smaller value of  $k \sim 0.03h\text{Mpc}^{-1}$  and no distinct “bump” at  $k = 0.05h\text{Mpc}^{-1}$ . Also, Peacock & West (1992) and Jing & Valdarnini (1993) find a break in the Abell cluster power spectrum near  $k = 0.05h\text{Mpc}^{-1}$ , but no excess peak in power. An excellent review of the power spectra for different galaxy species can be found in Einasto *et al.* (1999-hear-after E99). E99 determine a mean power spectrum for all galaxies for a large range in wavenumber. They do this by using the APM 2d power spectra on small scales, and by averaging over numerous samples on large scales and then normalizing to the APM 2d power.

If a peak in power near  $k \sim 0.05h\text{Mpc}^{-1}$  is a real feature of the power spectrum in general, most current models of structure formation (in the quasi-linear regime) become invalid (E99). Recently, Gramann & Suhonenko (1999) suggest that an inflationary scenario with a scalar field having a localized step-like feature can reproduce the power spectrum of clusters. However, in this work, we show that the peak in the cluster power spectrum is not present in cluster samples after excluding questionable data (such as  $R = 0$  Abell/ACO clusters and clusters with estimated redshifts).

Our aim in this paper is to provide an estimate for the power spectrum of Abell/ACO clusters that is based on a complete and fair sample. Both Retzlaff *et al.* and E97 use  $R = 0$  clusters in their determination of  $P(k)$ . Einasto *et al.* (1994) have argued that  $R = 0$  clusters do not contaminate studies of large-scale structure because the multiplicity of superclusters is independent of richness and the mean separation distances for  $R = 0$  and  $R \geq 1$  clusters are very similar. However,  $R = 0$  clusters were not cataloged in a systematic way and were never meant to be examined in a statistical manner due to their incompleteness (Abell 1958). In addition, many researchers have

found line-of-sight anisotropies in  $R = 0$  cluster samples (Sutherland 1988; Efstathiou *et al.* 1992; Peacock & West 1992). Therefore, the use of  $R = 0$  clusters in the determination of  $P(k)$  is highly suspect. E97 have also used a large number (435 out of 1305 clusters) of estimated redshifts in their determination of  $P(k)$ . We also suspect that E97 used a large number of cluster redshifts with only one measured galaxy. Miller *et al.* 1999a show that cluster velocities with one measured galaxy are off by over 2500 km s $^{-1}$  14% of the time. Of course, estimated redshifts are only accurate to at best 25%. Thus, the statistical certainty of any large-scale structure analyses based on the cluster samples with a large number of estimated or poorly determined redshifts must also be taken with caution.

## 2. THE CLUSTER SAMPLE

We examine Abell/ACO clusters throughout the entire sky excluding the galactic plane *i.e.*  $|b| > 30^\circ$ . We only consider  $R \geq 1$  clusters (with measured redshifts) since they were defined by Abell (1958) as members of his statistically complete sample. Recently, Miller *et al.* (1999a,b) examine similar subsets of  $R \geq 1$  clusters for projection effects, line-of-sight anisotropies, and spatial correlations. We summarize their results below.

The Abell/ACO  $R \geq 1$  cluster dataset has significant advantages over other cluster samples (including those with  $R = 0$  clusters as well as APM clusters). With the advent of multi-fiber spectroscopy, nearly all rich Abell/ACO clusters within  $z = 0.10$  now have multiple galaxy determined redshifts (Slinglend *et al.* 1998; Katgert *et al.* 1996). Multiple redshifts have allowed for more accurate determinations of the extent of projection effects and Miller *et al.* 1999a report that at most, 10% of Abell/ACO clusters suffer from moderate to severe foreground/background contamination. The lack of projection effects for  $R \geq 1$  clusters is also apparent from the 89% X-ray emission detection rate by Voges *et al.* 1999. Miller *et al.* (1999a,b) also show that there is very little line-of-sight anisotropy in the  $R \geq 1$  Abell/ACO cluster samples - comparable to the APM cluster catalog (Dalton *et al.* 1994). This is in sharp contrast to  $R \geq 0$  samples and even some modern X-ray selected/confirmed cluster samples.

Vogeley (1998) recently pointed out how galactic extinction could add “false” power to structure analyses based on large galaxy samples (such as the Sloan Digital Sky Survey). While clusters should not be affected as strongly as individual galaxies, it is still worth examining extinction effects within our cluster sample. In 1996, Nichol and Connolly used the Stark *et al.* 1992 HI maps to report that some samples of Abell clusters significantly anti-correlate with regions of high galactic neutral hydrogen density. Recently, Schlegel, Finkbeiner, and Davis (1998) have created HI extinction maps of the entire sky with much greater resolution than the Stark HI maps. We use these new maps to re-examine and confirm the Nichol and Connolly results. We also examine a volume-limited ( $z = 0.10$ ) sample of Abell/ACO clusters. Using a Kolmogorov-Smirnov (K-S) test, we compare the E(B-V) extinctions for positions centered on the Abell/ACO clusters to E(B-V) extinctions for several thousand randomly selected positions. We find that the probability that our clusters were drawn from a random selection of E(B-V) extinctions is 10%. In other words, the average extinction within our Abell/ACO clusters

is smaller than for the random positions, but not significantly so. For comparison, Nichol and Connolly found only a 2% probability that the Postman, Huchra, and Geller Abell/ACO clusters (with  $|b| \geq 30^\circ$  and  $R \geq 1$ ) were drawn from a random sampling of E(B-V) extinctions. The effect that galactic extinction would have on a power spectrum should not be as strong for clusters as it would be for galaxies. Cluster galaxies have a wide range of magnitudes, and while some dimmer galaxies within a cluster may be missed due to extinction, the majority of bright galaxies will still be counted. When we created our volume-limited samples, we are including those clusters that appear dim as a result of galactic extinction (as opposed to a magnitude-limited survey which would exclude those clusters). Therefore, the lack of statistically significant evidence that our clusters are corrupted by extinction and the use of a volume-limited sample (with  $|b| \geq 30^\circ$ ), convinces us that we can ignore any extinction effects in our analyses.

An additional argument for the completeness of  $R \geq 1$  Abell/ACO clusters is provided by their spatial number density as shown in Figure 1. We use clusters of all magnitudes and use the same methods as Miller *et al.* (1999a) to calculate and bin the cluster number densities. In the southern hemisphere, we have excluded all clusters with  $N_{gal} < 54$  (as listed in the ACO catalog). This accounts for selection differences between the Abell and ACO catalogs (see Miller *et al.* 1999a for further details). We find  $\bar{n}_c = 8.7 \pm 1.8 \times 10^{-6} h^3 \text{Mpc}^{-3}$  for the north and  $\bar{n}_c = 8.7 \pm 4.0 \times 10^{-6} h^3 \text{Mpc}^{-3}$  for the south. The greater scatter in the Southern hemisphere is due to the small number of clusters (82 between  $-90^\circ \leq \delta \leq -27^\circ$  and within  $z = 0.10$ ). Notice that both the Northern and Southern hemispheres have a nearly constant density out to  $z = 0.10$  and that the density in the north only drops by a factor of 0.58 out to  $z = 0.14$ . Using cluster redshifts from the literature as well as  $\sim 100$  as yet unpublished redshifts from the MX Survey Extension (Miller *et al.* 1999c), we have created a sample of 545  $R \geq 1$  Abell/ACO clusters with  $|b| \geq 30^\circ$ . We exclude any cluster beyond  $z = 0.10$  in the south ( $\delta \leq -27^\circ$ ) and beyond  $z = 0.14$  in the north ( $\delta \geq -27^\circ$ ). Only  $\sim 10\%$  of our cluster redshifts are based on one measured redshift. This is the largest cluster sample compiled to date for large-scale structure analyses. The survey volume covers  $1.2 \times 10^8 h^{-3} \text{Mpc}^3$  and is nearly four times larger than the APM cluster survey (Dalton *et al.* 1994) and the Retzlaff *et al.* (1998) Abell/ACO survey. We calculate distances to the clusters using a Friedman Universe with  $q_0 = 0$  and  $H_0 = 100 \text{ km s}^{-1} \text{ Mpc}^{-1}$ .

When a cluster dataset goes as deep as the one used here, we must also be concerned with observational biases. In other words, we need to be confident that all regions of the sky have been observed nearly equally. We address this concern figuratively in Figure 2. In this sky plot (in galactic coordinates), we show Abell clusters with  $z = 0.10$  (filled circles), Abell clusters within  $0.10 < z \leq 0.14$  (open circles), and ACO clusters within  $z = 0.10$  (stars). We can divide the sky into quadrants with two sections in the north and two in the south (each separated at  $l = 180^\circ$ ) and examine nearby ( $z \leq 0.10$ ) and distant ( $0.10 < z \leq 0.14$ ) clusters separately. From Figure 2, we see reasonably fair coverage throughout the entire sky in both redshift ranges (recall that the south-

ern right quadrant only goes to  $z = 0.10$ ). Quantitatively, we present in Table 1 the number of clusters available in each quadrant cataloged by Abell/ACO, and the number of clusters observed in each quadrant. Note that the fractional coverages in each of the sections are very similar. The mean fractional coverage (including both near and far quadrants) is  $0.138 \pm 0.019$ , so that the number of clusters within the more distant, northern right quadrant is only  $1.5\sigma$  smaller than the mean. Table 1 provides clear evidence that the sky coverage for our cluster sample is not observationally biased towards certain regions.

After accounting for projection effects, line-of-sight anisotropies, X-ray identifications, HI column density variations, a constant number density, and fair sky coverage, this is the largest, most complete, and fairly sampled distribution of matter in the local Universe. We assume that clusters are biased tracers of mass (Kaiser 1986; Peacock & Dodds 1994). In all further analyses, we use our larger cluster sample (to  $z = 0.10$  in the South and to  $z = 0.14$  in the North). We model our redshift selection in the Northern hemisphere to account for the small dropoff in density beyond  $z = 0.10$ .

### 3. METHODS AND ANALYSES

We utilize two different methods to estimate  $P(k)$  in redshift-space. Both methods follow the same basic idea: directly sum the plane wave contributions from each cluster, account for appropriate weights and the shape of the volume, compute the square of the modulus of each mode and subtract off the shot noise. The resultant power spectrum is the estimated variance of the density contrast  $|\delta(k)|^2$ . The power spectrum is valid only to some limiting value,  $k_{min}$ , which is constrained by the size and shape of the volume examined. The differences between the two methods arise when accounting for the weighting scheme and the shape of the volume. We also point out that Tegmark *et al.* (1998) have recently presented an alternative method for measuring  $P(k)$  for large datasets (such as the Sloan Digital Sky Survey). As discussed in detail in Tegmark *et al.*, they advocate the use of standard Fourier techniques on small scales, a pixelized quadratic matrix method on large-scales, and also a Karhunen - Loeve (KL) eigenmode analysis to probe redshift-space anisotropies. While the Tegmark *et al.* power spectrum estimation method is undoubtedly more refined than the methods used here, we are more interested in comparing results from the most commonly used techniques (and also allowing our results to be compared to previous cluster  $P(k)$  measurements).

The first method we use is described in LCRS and Fisher *et al.* 1993. Recently, this method was also used and described by Retzlaff *et al.* 1998. Briefly, the estimated power spectrum convolved with the window function can be written as follows:

$$\hat{P}_a(k) = \frac{V}{1 - |\hat{W}(k)|^2} [\hat{\Pi}(k) - \hat{S}]. \quad (1)$$

The first factor in Equation 1 accounts for the systematic under-estimation of  $P(k)$  at small values of  $k$  due to normalization biases and the shape of the window (Peacock & Nicholson 1991). The first term in brackets,  $\hat{\Pi}$  is the Fourier transform of the variance in the density contrast,

$\delta(\mathbf{r})$ , or more simply, the estimated power (convolved with the window function) including shot noise. Finally,  $\hat{S}$  is the power due to the shot noise of a discreet data sample. All quantities with a hat denote estimated values. In practice, we calculate  $\hat{W}(k)$  separately for as many points as is feasible (in this case  $3 \times 10^5$  random points) and average over 1000 directions of  $k$ . The weights for each cluster originate in the estimation of the density contrast,

$$\hat{\delta}(r) = \frac{1}{n} \sum_i \frac{\delta^3(\mathbf{r} - \mathbf{r}_i)}{\phi(r_i)} - 1 \quad (2)$$

where  $\phi(r) = \psi(b)\varphi(z)$  is the selection function which accounts for galactic obscuration and redshift selection. We use  $\psi(b) = 10^{\gamma(1-csc|b|)}$  with  $\gamma = 0.32$  for the latitude selection function. We use  $\varphi(z) = 1$  for clusters within  $z = 0.10$  and  $\varphi = 0.58$  for clusters with  $0.10 < z \leq 0.14$ .

The second method we use was derived by Feldman, Kaiser, & Peacock (1994-hereafter FKP). TED96 use a very similar approach in their analysis of APM clusters. Here, the power spectrum is:

$$\hat{P}_b(k) = |F(\mathbf{k})|^2 - P_{shot} \quad (3)$$

where  $F(k)$  is the Fourier transform of the normalized and weighted galaxy fluctuation field:

$$F(\mathbf{r}) = \frac{\mathbf{w}(\mathbf{r})[\mathbf{n}_c(\mathbf{r}) - \alpha \mathbf{n}_s(\mathbf{r})]}{\int d^3r \bar{n}^2(\mathbf{r}) \mathbf{w}^2(\mathbf{r})^{1/2}} \quad (4)$$

In these equations,  $n_c$  and  $n_s$  represent the number densities of the cluster sample and a randomly generated synthetic catalog respectively. The number of points we use in the random catalog is 20 times that of the real data so  $\alpha = \frac{1}{20}$  (we note that there is no difference in the power spectrum results for random catalogs with 40 or even 80 times as many points).  $P_{shot}$  is again, the power due to shot noise from a discreet sample. The weights for the individual clusters (real and synthetic) are determined from

$$w_o(r) = \frac{1}{1 + \bar{n}(r)P(k)}. \quad (5)$$

The weighting scheme for  $P_b(k)$  depends on *a priori* knowledge of  $P(k)$  at all scales. We choose different values of  $P(k)$  ( $P_{init} = 5, 10, 20, 40 \times 10^4 h^{-3} \text{Mpc}^3$ ) for the cluster weights and find that there is little difference in the amplitude ( $\sim 1.5$  times) of  $P_b(k)$  between  $P_{init} = 5$  and  $40 \times 10^4 h^{-3} \text{Mpc}^3$  and so we adopt  $P_{init} = 20 \times 10^4 h^{-3} \text{Mpc}^3$  in all further  $P_b(k)$  results (see Figure 3a). We calculate errors on  $P_b(k)$  using those methods of FKP (equation 2.4.6). We present  $P_a(k)$  and  $P_b(k)$  in Figure 3b. The lack of difference between  $P_a(k)$  and  $P_b(k)$  is a direct result of the stability of the methods and the well defined number density and semi-regular volume of the cluster sample.

### 4. DISCUSSION

There are two striking results regarding the power spectrum of rich Abell/ACO clusters. (1) There is no statistically significant peak in the power spectrum as has been reported in E97 and Retzlaff *et al.* (1998) and (2) there is clearly increasing power to very large scales

( $k = 0.02h\text{Mpc}^{-1}$  or  $\sim 300h^{-1}\text{Mpc}$ ). In addition, there is a flattening of the power spectrum on scales as large as we can accurately probe ( $k = 0.009h\text{Mpc}^{-1}$ ). In past analyses of the power spectrum, most authors have reported the (weak) detection of a turnover in the power spectrum (see section 1). However, the turnover has always occurred very near the largest scales accessible in their volumes. The smallest wavenumber  $k_{min}$ , that can be used in such an analysis is determined by  $\langle|\hat{W}(\mathbf{k})|^2\rangle = 0.1$ . If we use a top-hat window function where the radius is the weighted average,  $R_A$ , of the Northern (90% of volume) and Southern (10% of volume), we have  $k = \frac{3.1}{R_A}$  and  $R_A = 390h^{-1}\text{Mpc}$ . Thus,  $k_{min} = 0.008h\text{Mpc}^{-1}$  if the window function was exactly a top-hat (Peacock & West (1992)). Since the window function is actually comprised of two different size top-hats, it is more appropriate to look at the Monte-Carlo-determined window function,  $\langle|\hat{W}(\mathbf{k})|^2\rangle$ , used in  $P_a(k)$ . This is presented in Figure 4, where it is clear that  $k_{min} = 0.009h\text{Mpc}^{-1}$ . We have adopted this more conservative limit in our analysis. Regardless of which  $k_{min}$  we adopt, the power that we detect on scales  $0.01 < k \leq 0.05h\text{Mpc}^{-1}$  is not an artifact created by the convolution of  $P(k)$  with the window function. The power spectrum is roughly linear on scales  $0.02 \leq k < 0.10h\text{Mpc}^{-1}$  with  $P(k) \propto k^{-1.4}$ .

The differences between our cluster sample power spectrum and other previous cluster sample analyses are shown in Figure 5. Here, we show  $P(k)$  for the less rich APM clusters of TED98. The higher amplitude for our sample of  $R \geq 1$  clusters is expected according to hierarchical clustering schemes (Kaiser 1986) and larger bias found in richer clusters (see Peacock and Dodds 1994). We also have recalculated the Retzlaff *et al.* (1998) Abell/ACO cluster sample using the methods for  $P_a(k)$ . We do this in part as a check on our methods and also to independently confirm their results of a peak near  $k = 0.05h\text{Mpc}^{-1}$  and a turnover thereafter. The Retzlaff *et al.* sample includes all Abell/ACO clusters within  $240h^{-1}\text{Mpc}$  and outside  $|b| \geq 30^\circ$ . We find 412 clusters which meet this criteria (compared to their 417 clusters- the difference we attribute to minor variations in a few cluster redshifts near the survey boundaries). Our results, not surprisingly, are identical to those published in Retzlaff *et al.* (1998) since our method for determining  $P_a(k)$  is identical to theirs. For this determination of  $P_a(k)$  (*i.e.* using  $R = 0$  clusters and a much smaller volume), we also see a peak in the power spectrum at  $k = 0.05h\text{Mpc}^{-1}$  and a turnover thereafter. As pointed out by Retzlaff *et al.*, this peak is not statistically significant and we find that volume effects are compounding the evidence by finding a “false” turnover in  $P(k)$ . To see how the size of the volume affects the analysis, we also plot  $P(k)$  for our much smaller  $z = 0.10$  limited sample (which is very similar in size to the Retzlaff *et al.*  $z \leq 0.85$  sample, but contains only  $R \geq 1$  clusters). In this case, our volume is nearly one third that of our larger sample and so we expect our minimum wavenumber to be  $k_{min} \sim 0.03$ . Figure 5 clearly shows a decrease in power which becomes evident near  $k_{min}$ . Figure 5 also indicates that the shapes of  $P(k)$  for these different cluster samples are similar in the range  $0.04 \leq k \leq 0.10h\text{Mpc}^{-1}$ .

We also compare our power spectrum results to those of linear theory created by CMBFAST (Seljak & Zeldar-

riaga 1996). We consider two Cold Dark Matter (CDM) variants, open and with a vacuum density ( $\Lambda\text{CDM}$ ), and a Mixed Dark Matter (MDM) model. For the CDM cases, we choose  $\Omega_b = 0.02$ , in accordance with Schramm & Turner (1998). For the open case, we choose  $\Omega_0 = \Omega_b + \Omega_{CDM} = 0.2$  in accordance with Bahcall (1997). For the  $\Lambda\text{CDM}$  model, we choose  $\Omega_{CDM} = 0.18$  and  $\Omega_{vacuum} = 0.80$  so that  $\Omega_b + \Omega_{CDM} + \Omega_{vacuum} = 1$ . For the MDM model, we choose  $H_0 = 50\text{km s}^{-1}\text{Mpc}^{-1}$  with  $\Omega_b = 0.05$ ,  $\Omega_{CDM} = 0.35$  and  $\Omega_\nu = 0.3$  (where  $\Omega_\nu$  is the massive neutrino density). The CMBFAST package normalizes the amplitude of generated spectra to the Bunn and White (1997) four-year COBE normalization. However, in this work, we are only concerned with the *shape* of the power spectrum. We are motivated by our assumption that clusters are biased tracers of the mass distribution and therefore the shape of the cluster power spectrum should be similar to that of the matter power spectrum. In Figure 6, we present the amplitude shifted linear models in comparison to our empirically determined power spectra. As a result of the known similarities in the shapes of the  $\Lambda\text{CDM}$  models and low matter density open CDM models, we find that both fit the shape of the rich Abell/ACO cluster power spectrum to  $k_{min} = 0.009h\text{Mpc}^{-1}$  or  $700h^{-1}\text{Mpc}$  extremely well. On the largest scales, the MDM model lacks power over a wide range of  $k$  ( $0.009 \leq k \leq 0.03h\text{Mpc}^{-1}$ ) to match our cluster data. TED98 found that  $\Lambda\text{CDM}$  linear models did not have enough power on large scales to match the APM cluster power spectrum. Instead, they find a much better fit for a mixed dark matter (MDM) model. We point out that the  $\Lambda\text{CDM}$  model in Figure 7 of TED98 does provide an excellent fit to the APM cluster data if their last data point at  $k = 0.02h\text{Mpc}^{-1}$  (where the error is rather large) is excluded.

## 5. CONCLUSION

The agreement between the shapes of  $P(k)$  for the four different samples shown in Figure 5 provides further evidence that clusters are excellent tracers of mass on large scales. However, previous analyses of the cluster power spectrum have been plagued by three major problems: (1) uncertainties in the number density, (2) small volumes, and (3) irregularly shaped volumes. The sample analyzed in this work greatly improves upon each of these difficulties. Our Abell/ACO sample has a nearly constant number density throughout the entire volume. This is in stark contrast to most other sparse tracer surveys (such as the QDOT *IRAS* survey power spectrum of FKP and the Retzlaff *et al.* Abell/ACO cluster sample). Along with the number density, the large size of the volume and the semi-regular shape of the double-cone geometry, all contribute significantly to a more accurate determination of  $P(k)$  on the largest scales. The reality of the power on scales  $200 - 300h^{-1}\text{Mpc}$  is also becoming evident observationally. Batuski *et al.* 1999 have recently discovered two filamentary superclusters in the constellation of Aquarius that are as long as  $75h^{-1}\text{Mpc}$  and  $150h^{-1}\text{Mpc}$ . As we peer at further into the local Universe, we continue to find structures on very large scales.

We have presented the redshift-space power spectrum for the largest galaxy cluster sample compiled to date. This sample has been examined extensively for projection

effects, anisotropies, and observational selection effects and found to be a fair and complete sampling of biased matter in the local Universe. The volume and shape of the survey provide accurate and robust measurements of  $P(k)$  over the wavenumber range  $0.009 \leq k \leq 0.100h\text{Mpc}^{-1}$ . From  $k = 0.10$  down to  $k = 0.05h\text{Mpc}^{-1}$ , we find a similar shape to the power spectrum compared to other cluster samples such as the APM cluster survey and a smaller sample of  $R \geq 0$  Abell/ACO clusters studied by Rettlaff *et al.* (1998). At smaller  $k$ , we do not find any statistically sig-

nificant features in  $P(k)$ . The shape of our cluster power spectrum appears to flatten around  $k = 0.02h\text{Mpc}^{-1}$ , but unlike previous cluster  $P(k)$  analyses, we do not find any strong evidence for a turnover. We find that  $\Lambda\text{CDM}$  and low  $\Omega_0$  CDM linear models provide excellent fits to the rich cluster power spectrum.

**Acknowledgments** The authors wish to thank Adrian Melott for helpful conversations. CM was funded in part by NASA-EPSCoR through the Maine Science and Technology Foundation.

## REFERENCES

Abell, G. O. 1958, ApJS, 3, 211  
 Abell, G. O., Corwin, H. G., Olowin, R. P. 1989, ApJS, 70, 1 (ACO)  
 Bahcall, N. 1997, in *Critical Dialogues in Cosmology*, ed. N. Turok, World Scientific, Singapore, 221  
 Batuski, D.J., Miller, C.J., Slinglend, K.A., Balkowski, C., Maurogordato, S., Cayatte, V., Felenbok, P., and Olowin, R. 1999, ApJ, 520, 491  
 Broadhurst, T.J., Ellis, R.S., Koo, D.C., & Szalay, A.S. 1990, Nature, 343, 726  
 Bunn, E.F. & White, M. 1997, ApJ, 480, 6  
 Dalton, G.B., Croft, R.A.C., Efstathiou, G., Sutherland, W.J., Maddox, S.J., and Davis, M. 1994, MNRAS, 271, 47  
 Efstathiou, G., Dalton, G.B., Maddox, S.J., & Sutherland, W. 1992, MNRAS, 257, 125  
 Einasto, J., Einasto, M., Gottlöber, S., Müller, V., Saar, V., Starobinsky, A.A., Tago, E., Tucker, D., Andernach, H., & Frisch, P. 1997, Nature, 385, 139 (E97)  
 Einasto, J., Einasto, M., Tago, E., Starobinsky, A.A., Atrio-Barandela, F., Müller, V., Knebe, A., & Cen, R. 1999, ApJ, 519, 469 (E99)  
 Frisch, P. 1997, Nature, 385, 139 (E97)  
 Einasto, M., Einasto, J., Tago, E., Dalton, G.B., & Andernach, H. 1994, MNRAS, 269, 301  
 Feldman, H.A., Kaiser, N., & Peacock, J.A. 1994, ApJ, 426, 23 (FKP)  
 Fisher, K.B., Davis, M., Strauss, M.A., Yahil, A., & Huchra, J.P. 1993, ApJ, 402, 42  
 Gatzañaga, E. & Baugh, C.M. 1998, MNRAS, 294, 229  
 Gramann, M. & Suhhonenko, I. 1999, ApJ, 519, 433  
 Jing, Y.P. and Valdarnini, R. 1993, ApJ, 406, 6  
 Kaiser, N. 1986, MNRAS, 222, 323  
 Katgert, P., Mazure, A., Perea, J., den Hartog, R., Moles, M., Le Févre, O., Dubath, P., Focardi, P., Rhee, G., Jones, B., Escalera, E., Biviano, A., Gerbal, D., Giuricin, G. 1996, A & A, 310, 8  
 Landy, S.D., Shectman, S.A., Lin, H., Kirshner, R.P., Oemler, A.A., & Tucker, D. 1996, ApJ, 456, L1  
 Lin, H., Kirshner, R.P., Shectman, S.A., Landy, S.D., Oemler, A., Tucker, D.L., & Schechter, P.L. 1996, ApJ, 471, 617 (LCRS)  
 Miller, C.J., Batuski, D.J., Slinglend, K.A., & Hill, J.M. 1999a, ApJ, 523, 492  
 Miller, C.J., Ledlow, M.J. & Batuski, D.J. 1999b, MNRAS, submitted  
 Miller, C.J., Krughoff, K.S., Slinglend, K.A., Batuski, D.J., & Hill, J.M. 1999c (in preparation)  
 Nichol, R.C. & Connolly, A.J. 1996, MNRAS, 279, 521  
 Peacock, J.A. 1997, MNRAS, 285, 885  
 Peacock, J.A. & Dodds, S.J. 1994, MNRAS, 267, 1020  
 Peacock, J.A. & Nicholson, D. 1991, MNRAS, 253, 307  
 Peacock, J.A. & West, M.J. 1992, MNRAS, 259, 494  
 Postman, M., Huchra, J. P., & Geller, M. J. 1992, ApJ, 384, 404  
 Rettlaff, J., Borgani, S., Gottlöber, S., Klypin, A., & Müller, V. 1998, NewA, 3, 631  
 Schlegel, D.J., Finkbeiner, D.P., & Davis, M. 1998, ApJ, 500, 525  
 Schramm, D.N. & Turner, M.S. 1998, Rev. Mod. Phys., 70, 303  
 Seljak, U. & Zaldarriaga, M. 1996, ApJ, 469, 437  
 Slinglend, K.A., Batuski, D.J., Miller, C.M., Haase, S., Michaud, K., & Hill, J.M. 1998, ApJS, 115, 1  
 Stark, A.A., Gammie, C.F., Wilson, R.W., Bally, J.L., Linke, R.A., Heiles, C., & Hurwitz, M. 1992, ApJS, 79, 77  
 Sutherland, W. 1988, MNRAS, 234, 159  
 Tadros, H., & Efstathiou, G. 1996, MNRAS, 282, 1381 (TE96)  
 Tadros, H., Efstathiou, G., & Dalton, G. 1998, MNRAS, 296, 995 (TED98)  
 Vogeley, M. 1998, in *The Evolving Universe*, Kluwer Academic Publishers, p. 395  
 Voges, W., Ledlow, M.J., Owen, F.N., & Burns J.O. 1999, AJ, submitted

TABLE 1  
Sky Coverage

$\ell$ range	$b$ range	$z$ range	Number (all $z$ ) cataloged	Number observed	Fraction
$0^\circ \leq \ell < 180^\circ$	$30^\circ \leq b \leq 90^\circ$	$z \leq 0.10$	636	80	0.1257
$0^\circ \leq \ell < 180^\circ$	$30^\circ \leq b \leq 90^\circ$	$0.10 < z \leq 0.14$	636	86	0.1352
$180^\circ \leq \ell < 360^\circ$	$30^\circ \leq b \leq 90^\circ$	$z \leq 0.10$	503	78	0.1550
$180^\circ \leq \ell < 360^\circ$	$30^\circ \leq b \leq 90^\circ$	$0.10 < z \leq 0.14$	503	52	0.1034
$0^\circ \leq \ell < 180^\circ$	$-90^\circ \leq b \leq -30^\circ$	$z \leq 0.10$	608	95	0.1563
$0^\circ \leq \ell < 180^\circ$	$-90^\circ \leq b \leq -30^\circ$	$0.10 < z \leq 0.14$	608	84	0.1382
$180^\circ \leq \ell < 360^\circ$	$-90^\circ \leq b \leq -30^\circ$	$z \leq 0.10$	492	75	0.1524

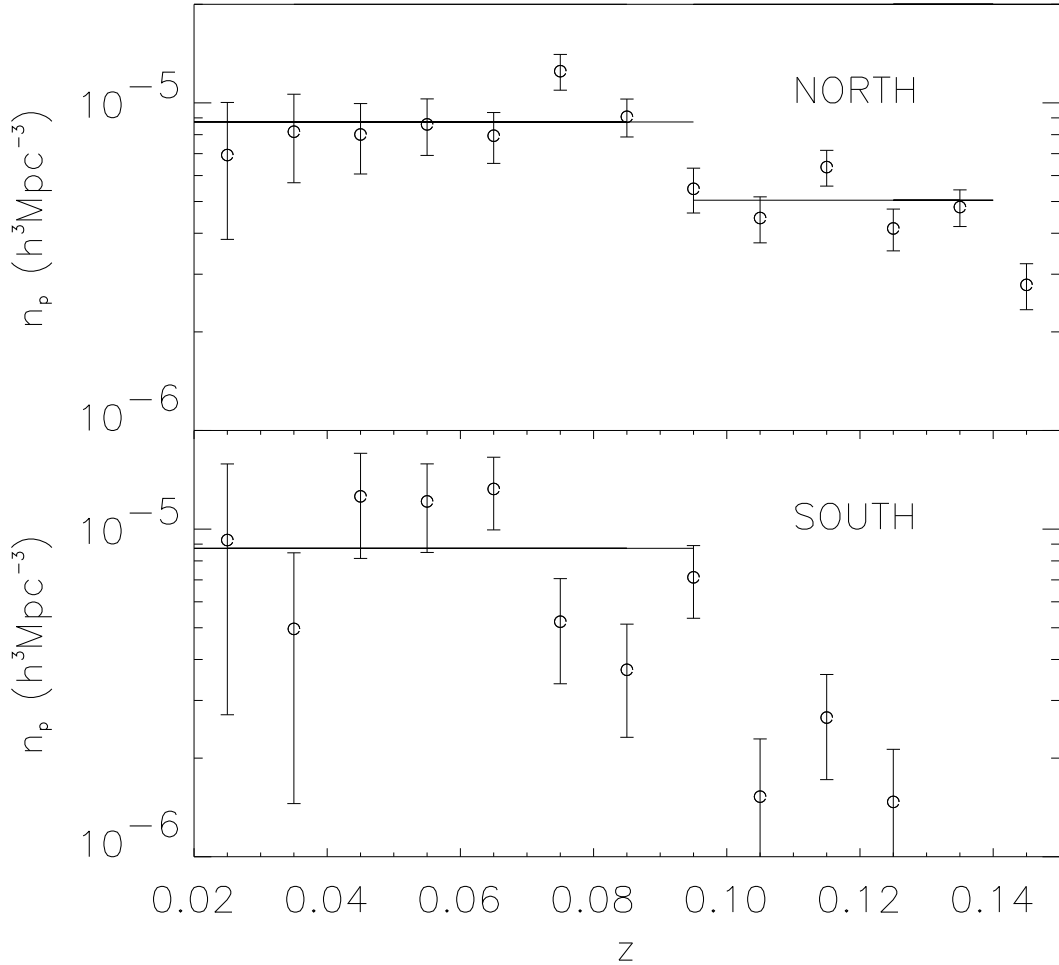


FIG. 1.— In the **top** panel we show the number density in the Northern Hemisphere ( $-27^\circ \leq \delta \leq 90^\circ$ ). This northern sample contains 453  $R \geq 1$  Abell (1958) clusters within  $z = 0.14$ . The **bottom** panel shows the number density,  $n_c$ , for the Southern Hemisphere ACO (1989)  $R \geq 1$  clusters with  $N_{gal} \geq 54$ . This sample contains 82 clusters within  $z = 0.10$ . The solid lines are the average number densities as defined in the text.

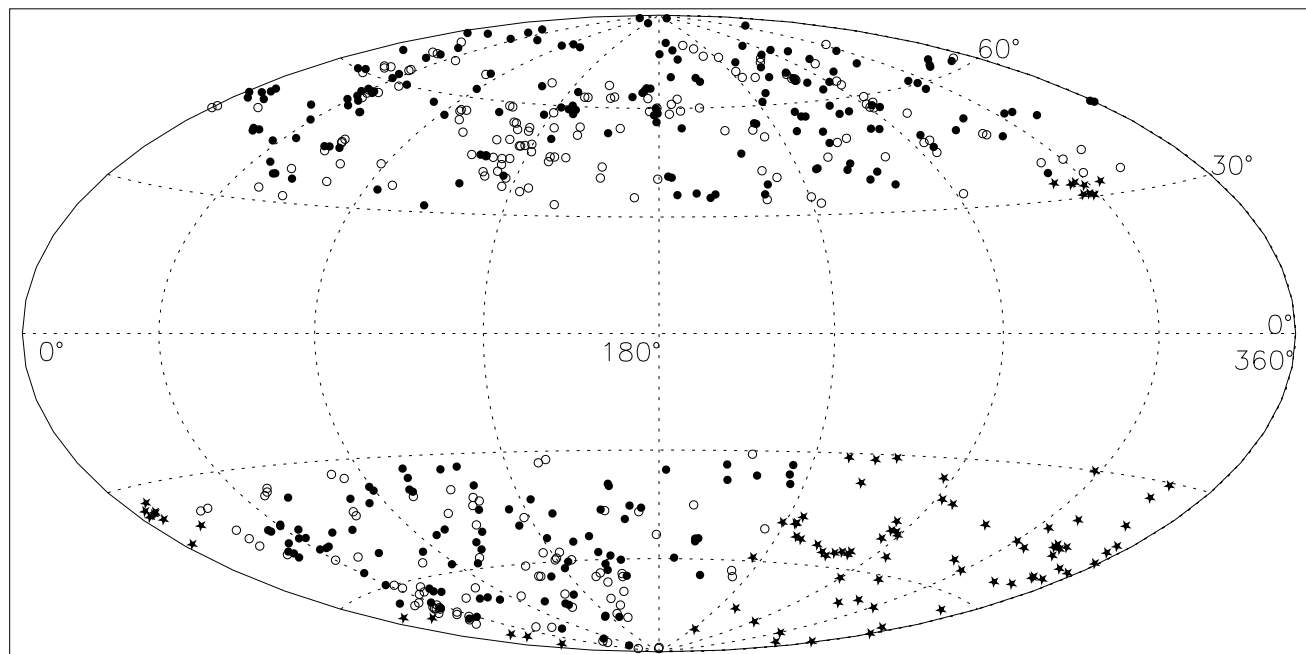


FIG. 2.— A Hammer-Aitoff projection sky-plot of all clusters used in the power spectrum analysis. Closed circles denote Abell (1958) clusters within  $z = 0.10$ , open circles denote Abell clusters with  $0.10 < z \leq 0.14$ , and stars indicate ACO (1989) clusters within  $z = 0.10$ .

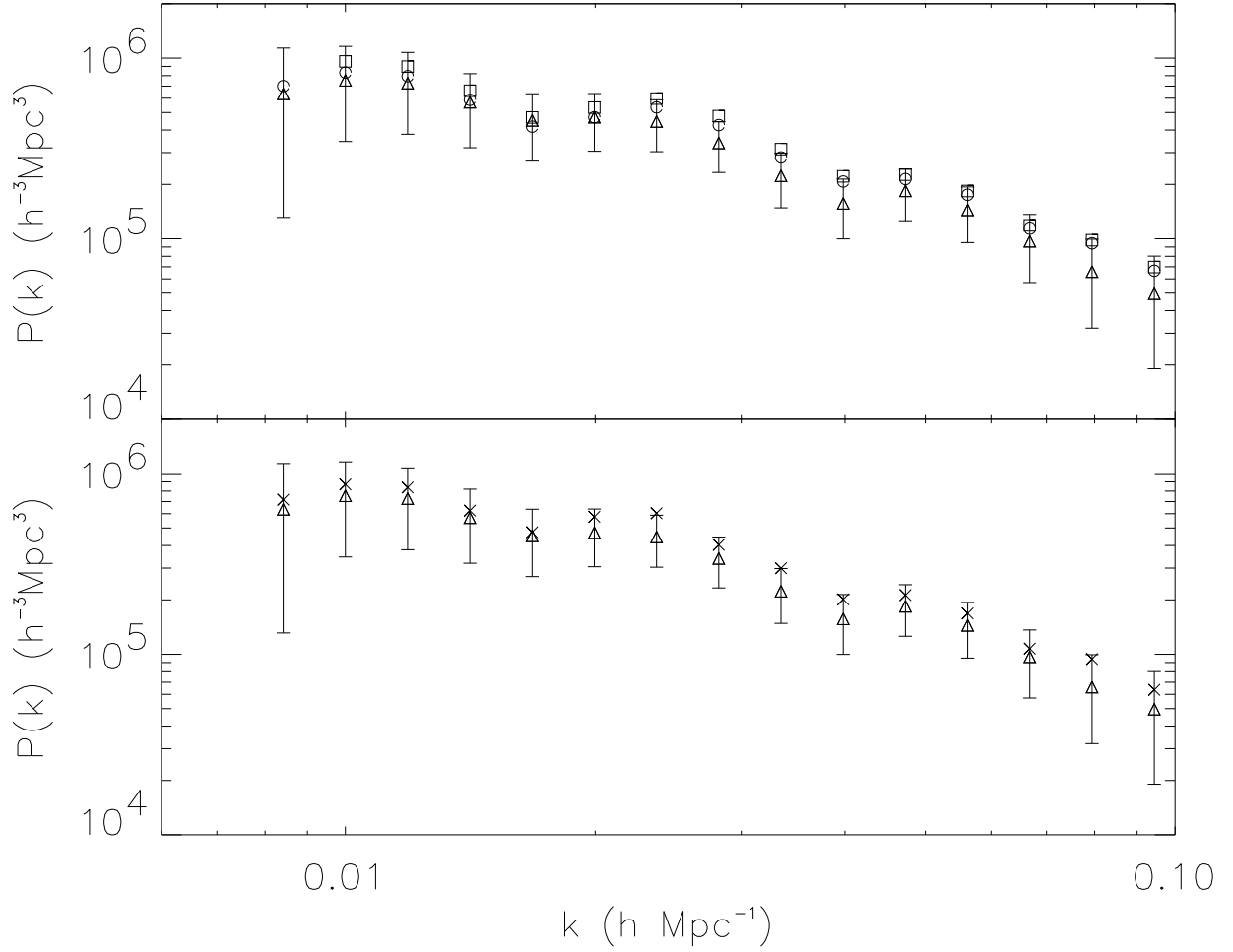


FIG. 3.— In the **top** panel we show  $P_b(k)$  calculated for different choices of  $(P_{init})$  in the weighting function. The order is 5, 10, 20, 40  $\times 10^4 h^3 \text{Mpc}^{-3}$  represented by circles, squares, triangles and diamonds respectively. The **lower** panel compares  $P_a(k)$  (crosses) to  $P_b(k)$  (triangles) where  $P_b(k)$  uses  $P_{init} = 20 \times 10^4 h^3 \text{Mpc}^{-3}$ . In both panels, the errors are calculated as described in the text on  $P_b(k)$  with  $P_{init} = 20 \times 10^4 h^3 \text{Mpc}^{-3}$

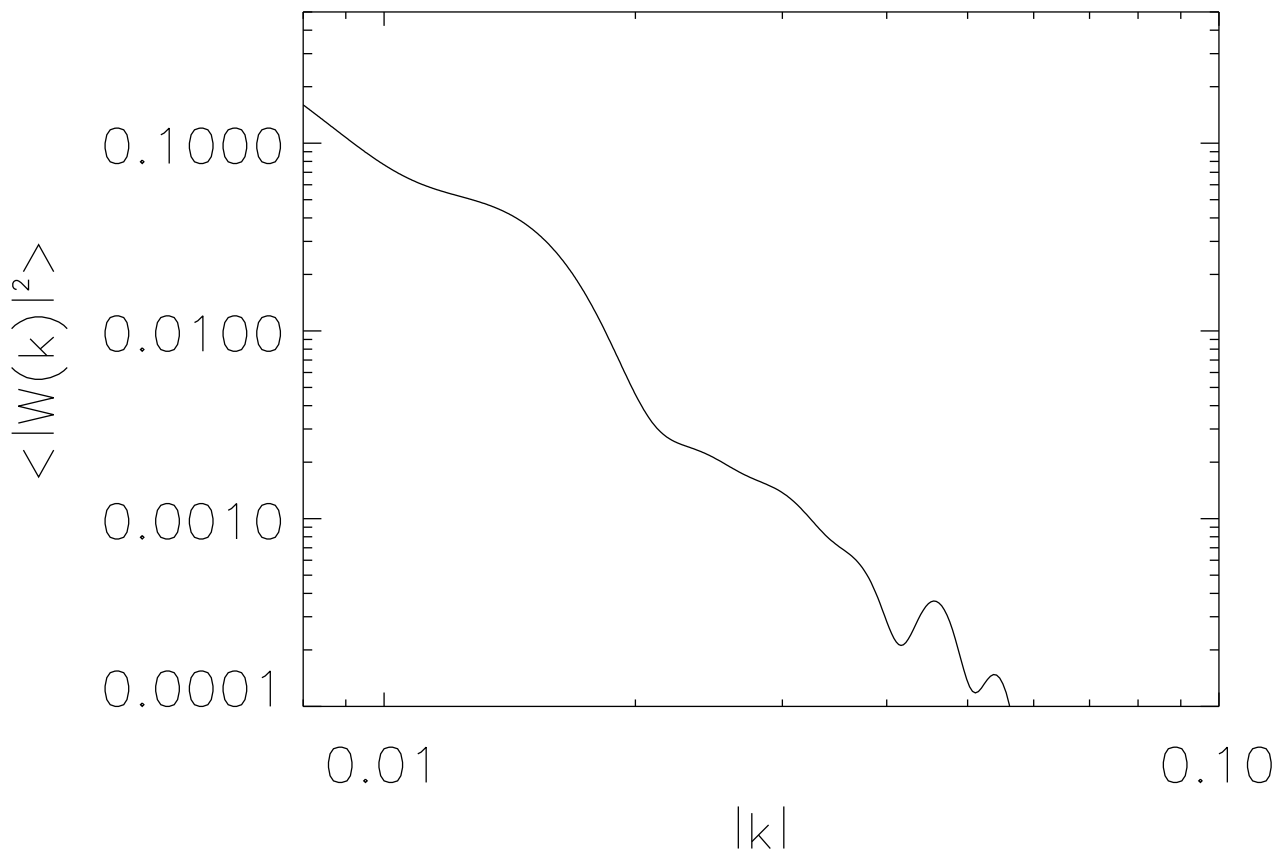


FIG. 4.— This is the window function,  $\langle |\hat{W}(\mathbf{k})|^2 \rangle$  used to calculate  $P_a(k)$ . We use 300000 points and 1000 random directions for each  $|\mathbf{k}|$  to estimate the Fourier transform of the window function.

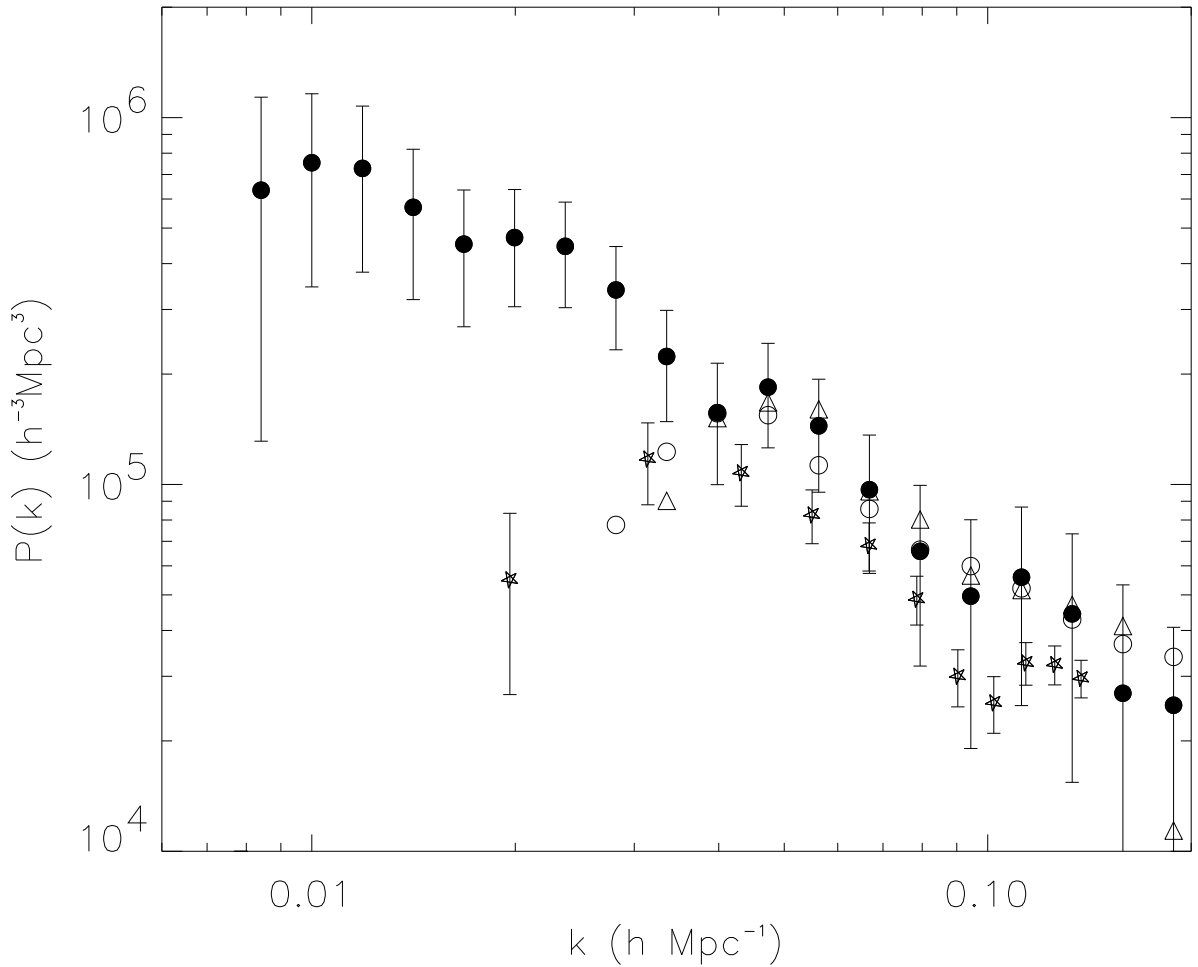


FIG. 5.— We compare  $P_b(k)$  for Abell/ACO clusters calculated in this work (solid circles) to the smaller Abell/ACO sample used by Retzlaff *et al.* (1998) (triangles) and the APM cluster sample power spectrum calculated by Tadros *et al.* (1998) (stars). The open circles are  $R \geq 1$  Abell/ACO clusters within  $z = 0.10$  (north and south). Note how significantly the power decreases as a result of the decreased volume size when compared to the larger sample (to  $z = 0.14$  in the north).

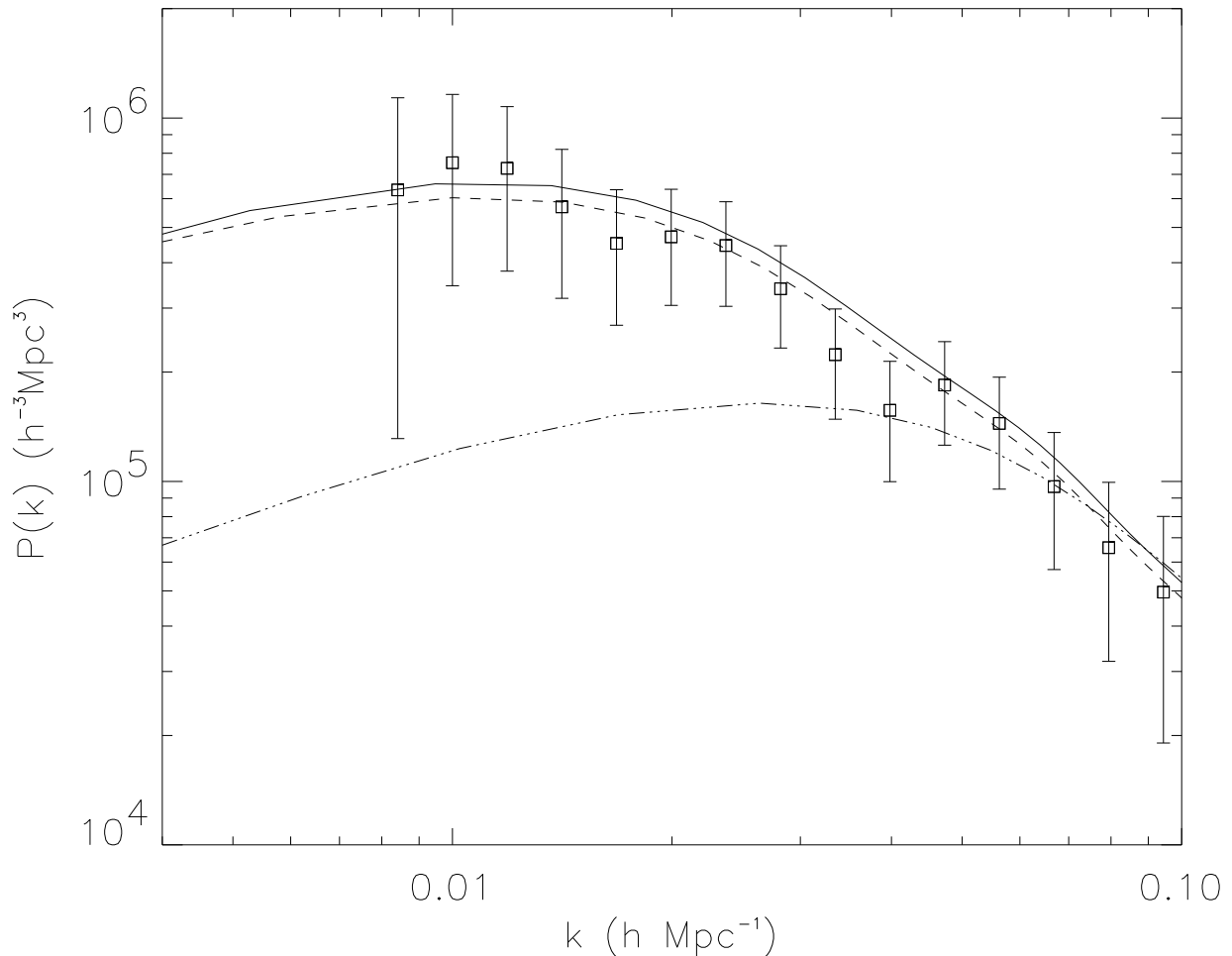


FIG. 6.— We compare  $P_b(k)$  to model liner power spectra for a mixed dark matter ( $\Omega_b = 0.05, \Omega_{CDM} = 0.65$  and  $\Omega_\nu = 0.3$  with  $H_0 = 50 \text{ km s}^{-1} \text{ Mpc}^{-1}$  **dashed-dot**), open ( $\Omega_b = 0.02, \Omega_{CDM} = 0.18$  with  $H_0 = 100 \text{ km s}^{-1} \text{ Mpc}^{-1}$  **dashed**), and lambda ( $\Omega_b = 0.02, \Omega_{CDM} = 0.18, \Omega_{vacuum} = 0.80$  **solid**) CDM models.